Contribution from the Departments of Chemistry, University of Notre Dame, Notre Dame, Indiana 46556, and University of Southern California, Los Angeles, California 90089-0744

Metalloporphyrin π-Cation Radicals. Intermolecular Spin Coupling in Zinc Tetraphenylporphyrin Derivatives

Hungsun Song,[1] Nigam P. Rath,[1] Christopher A. Reed,*[,2] and W. Robert Scheidt*[,1]

Received December 28, 1988

The solid-state magnetic susceptibilities of the $S = {}^1/_2$ [Zn(TPP•)($OClO_3$)] π-cation-radical system have been measured for different crystalline phases. The temperature-dependent diminution of magnetic moment is interpreted in terms of intermolecular spin coupling. The differing temperature dependencies of the moments for different crystalline phases show that the phenomenon is structure dependent. Crystal structure determinations of two different crystalline polymorphs of [Zn(TPP•)($OClO_3$)], isolated as bis(dichloromethane) solvates, show solid-state interactions between pairs of radicals. We provide detailed magnetic measurements for one of these phases and for the unsolvated crystalline phase previously reported by Spaulding et al. (*J. Am. Chem. Soc.* **1974**, *96*, 982) and interpret the differences in moments. Both of the solvated [Zn(TPP•)($OClO_3$)] species show "tighter" cofacial dimer structures than that observed in the Spaulding phase, and this correlates with increased antiferromagnetic coupling. Further, the differing intermolecular interactions have small but significant effects on metal atom displacement and axial bond lengths. Both new complexes are five-coordinate with an axially coordinated perchlorate ion. Average Zn–N distances are 2.060 (14) and 2.075 (7) Å in the two forms of the complex; Zn–O bond distances are 2.129 (3) and 2.139 (4) Å. Crystal data for form 1: monoclinic, $ZnCl_5O_4N_4C_{46}H_{32}$, a = 13.503 (4) Å, b = 18.582 (5) Å, c = 17.236 (8) Å, β = 109.32 (3)°, V = 4081.2 Å^3, Z = 4, space group $P2_1/c$. Crystal data for form 2: monoclinic, $ZnCl_5O_4N_4C_{46}H_{32}$, a = 12.485 (3) Å, b = 17.141 (11) Å, c = 19.443 (5) Å, β = 95.29 (2)°, V = 4143.1 Å^3, Z = 4, space group $P2_1/n$. All structural data were obtained at 118 K.

In recent work on metalloporphyrin π-cation radicals, notable structure-dependent differences have been observed in the intramolecular magnetic coupling that occurs between metal and porphyrin spins. Iron(III) and copper(II) porphyrins are exemplary in this regard,[3,4] revealing two distinct types of metal/ligand magnetic coupling: ferromagnetic and antiferromagnetic. We suggested that ferromagnetic coupling arises when the magnetic orbital(s) of the metal and the porphyrin π-cation-radical orbital are orthogonal. Such orthogonality is the result of a symmetry requirement that arises when the porphyrin core is in a strictly planar environment and the metal is located at the center (D_{4h} symmetry). Antiferromagnetic coupling arises in lower symmetry systems where the metal and ligand magnetic orbitals are not strictly forbidden by symmetry to overlap.

However, implicit in these arguments was a separation of intermolecular effects from intramolecular effects. For the ferromagnetically coupled systems there is no ambiguity. Complexes of known or presumed D_{4h} symmetry such as [Fe(TPP•)($OClO_3$)$_2$][5] and [Cu(TMP•)]$^+$[4] are magnetically isolated in the solid state and have no significant intermolecular interactions. Indeed, it is the lack of aggregation that probably leaves these metalloporphyrins free to adopt planar structures of D_{4h} symmetry. The two axial perchlorate ligands in [Fe(TPP•)($OClO_3$)$_2$] and the bulk mesityl groups in [Cu(TMP•)]$^+$ are apparently effective in preventing the face-to-face association that is common to many metalloporphyrin cation radicals. For the antiferromagnetically coupled systems, the spin coupling situation is not quite so straightforward. Both of the structurally characterized metalloporphyrin radical cations that display antiferromagnetic coupling, [Fe(TTP•)Cl]$^+$ and [Cu(TPP•)]$^+$, show pairwise cofacial association in the solid state. Thus, both intra- and intermolecular spin coupling could be present. A combination Mössbauer/susceptibility study[6] on [Fe(TPP•)Cl]$SbCl_6$ provides a good rational basis for partitioning the spin coupling into a strong intramolecular component ($|-J| > 200$ cm^{-1}) and a weak intermolecular component ($-J \approx 1$ cm^{-1}). The fully spin-coupling, diamagnetic [Cu(TPP•)]$^+$, however, does not lend itself so readily to a partitioning of intra- and intermolecular effects.

In this paper, we address the importance of intermolecular effects on magnetic coupling. The occurrence of aggregation in porphyrin π-cation radicals has been long recognized.[7] Indeed, in a recent review where the intermolecular interactions in all known solid-state structures of metalloporphyrin derivatives were surveyed, all four- and five-coordinate metalloporphyrin π-cation radicals were classified as displaying "dimer" formation.[8] Thus, there seems to be a strong driving force for dimeric association especially in the solid state. What are the effects of such dimerization on magnetic properties? Are such effects strongly structure dependent?

The conceptually simplest case in which to examine the possible effects of aggregation on magnetic properties is that of the d^{10} zinc derivative [Zn(Porph•)]$^+$, where the unpaired electron derives solely from the porphyrin radical. The solid-state structure of one crystalline phase of [Zn(TPP•)($OClO_3$)] has been previously investigated and the authors noted that pairs of [Zn(TPP•)($OClO_3$)] molecules are related by an inversion center to give "incipient dimers".[9] Thus, any deviation from the spin-only magnetic moment for this $S = {}^1/_2$ species should have an intermolecular basis. To our knowledge, however, no susceptibility measurements have been made on any [Zn(Porph•)]$^+$ radical. Our earliest magnetic susceptibility measurements of powder or microcrystalline samples of [Zn(TPP)(ClO_4)] and [Zn(TPP)($SbCl_6$)] showed magnetic moments that were depressed from their spin-only values and that decreased with decreasing temperature. This suggested antiferromagnetic coupling of a magnitude that would be useful for uncovering magnetostructural correlations.

In our work with magnetically interesting metalloporphyrin derivatives, we have emphasized susceptibility measurements on well-characterized solids since such measurements are the most reliable. We have always attempted to define the crystalline phase so that all measurements can be assessed in terms of known molecular structure and conformation and, in the present case, with well-defined intermolecular interactions. Determining the magnetic susceptibilities of precisely defined phases of [Zn(TPP•)($OClO_3$)] turned out to be surprisingly difficult. Our

(1) University of Notre Dame.
(2) University of Southern California.
(3) Gans, P.; Buisson, G.; Duée, E.; Marchon, J.-C.; Erler, B. S.; Scholz, W. F.; Reed, C. A. *J. Am. Chem. Soc.* **1986**, *108*, 1223–1234.
(4) Erler, B. S.; Scholz, W. F.; Lee, Y. J.; Scheidt, W. R.; Reed, C. A. *J. Am. Chem. Soc.* **1987**, *109*, 2644–2652.
(5) Abbreviations: TPP = tetraphenylporphyrinate; TMP = tetramesitylporphyrinate; TTP = tetra-*p*-tolylporphyrinate; Porph = general porphyrinate.
(6) Lang, G.; Boso, B.; Erler, B. S.; Reed, C. A. *J. Chem. Phys.* **1986**, *84*, 2998–3004.
(7) Furhop, J.-H.; Mauzerall, D. *J. Am. Chem. Soc.* **1969**, *91*, 4174–4181. Fajer, J.; Borg, D. C.; Forman, A.; Dolphin, D.; Felton, R. H. *J. Am. Chem. Soc.* **1970**, *92*, 3451–3459. Furhop, J.-H.; Wasser, P.; Riesner, D.; Mauzerall, D. *J. Am. Chem. Soc.* **1972**, *94*, 7996–8001.
(8) Scheidt, W. R.; Lee, Y. J. *Struct. Bonding (Berlin)* **1987**, *64*, 1–70.
(9) Spaulding, L. D.; Eller, P. G.; Bertrand, J. A.; Felton, R. H. *J. Am. Chem. Soc.* **1974**, *96*, 982–987.

0020-1669/89/1328-1839$01.50/0

attempts to prepare crystalline solids of [Zn(TPP•)($OClO_3$)] of the same phase as that reported by Spaulding et al.[9] were initially unsuccessful. Rather, we found that the reproducible preparation of crystalline [Zn(TPP•)($OClO_3$)] samples is a haphazard phenomenon. Ultimately, attempts to prepare crystalline [Zn(TPP•)($OClO_3$)] led to the identification of several different crystalline forms. We eventually found some degree of reproducibility in the experiments, but the phase(s) isolated are exquisitely sensitive to the experimental conditions. We have determined the crystal and molecular structure of two of these crystalline forms and we report cell constants for several additional phases. Eventually we were able to reproduce the Spaulding et al.[9] phase (termed by them as the β form) and obtain magnetic susceptibility data for this phase as well as one of the new phases. They show temperature-dependent decreases in their magnetic moments. We compare the magnetic susceptibility data in light of the crystal structure data and differences in intermolecular interaction of the molecules.

Experimental Section

General Data. UV–vis spectra were recorded on a Perkin-Elmer Lambda 4C spectrometer and IR spectra were recorded on a Perkin-Elmer 883 spectrometer. H_2TPP was prepared by the usual method.[10] Halocarbon solvents were distilled from CaH_2 and stored over molecular sieves. Thianthrenium perchlorate was prepared as previously described.[3] *Caution*! perchlorate salts can detonate spontaneously. Although no explosions were encountered in this work, precautions are warranted. Reactions involving ClO_4^- were always run on a small scale, and materials were not stored for long periods.

Synthesis and Crystallizations. All experiments were carried out under a blanket of dry argon in Schlenk ware or equivalent containers. ZnTPP (0.265 g, 0.391 mmol) and thianthrenium perchlorate (0.130 g 0.412 mmol) were stirred in 20 mL of dichloromethane for 30 min. The green solution was filtered, and crystallization was induced by careful layering of hexane above the solution. In all experiments, dark purple crystals were collected and washed with dry hexane. Typical yields were 70–85%. UV λ_{max} (CH_2Cl_2): 409 nm (Soret). IR (Nujol): 1277 s (TPP•), 1137 vs, b, 1027 s, 911 w cm^{-1} (ClO_4^-).

Depending on the precise nature of the crystallization experiment, different crystalline phases were isolated.

Method A. Initial crystallization experiments employed 100-mL Schlenk flasks (~3 cm diameter and 15 cm in length) with about 60 mL of dry hexane used for the hexane layer. The Schlenk flask was set aside and the hexane allowed to diffuse into the dichloromethane solution. The flask was maintained at various controlled temperatures that ranged from +5 to +22 °C or to −15 °C. Experiments lasted 1–2 weeks, the time required to achieve an essentially homogeneous solution.

Method B. This procedure used 100-mL serum-capped round-bottom flasks with 15 mL of dichloromethane solution and about 80 mL of dry hexane to induce crystallization. Temperatures were maintained at above ambient conditions (25–40 °C), and complete diffusion of the hexane usually occurred in less than 24 h. Crystals were usually harvested the next day and sorted by microscopic examination to achieve phase purity.

Magnetic Susceptibility. Measurements were performed on lightly ground samples (0.030 g) in an aluminum bucket on an SHE Model 905 SQUID susceptometer (at USC) at 10 kG. Samples synthesized at Notre Dame were shipped to Los Angeles at liquid N_2 temperatures in a biological dry shipper in order to avoid possible loss of solvent in transit. After the samples were thawed, sample grinding and mounting was done expeditiously (~10 min) to minimize solvent loss. Temperature-dependent experimental data were fitted as magnetic moments to the standard $2J$ spin Hamiltonian[11] for an $S = {}^1/_2$, $S = {}^1/_2$ system by using a least-squares program supplied to us by Dr. Peter Boyd. Complete data listings can be found in Tables SI and SII of the supplementary material for form 1 and the β phase, respectively.

Crystal Structure Determinations. Both crystalline phases of [Zn(TPP•)($OClO_3$)] were examined on an Enraf Nonius CAD4 diffractometer with the crystal temperature maintained at 118 K in order to avoid solvent loss.[12] Data collection crystals of both forms were freshly prepared, mounted on glass fibers with silicon grease, and quickly chilled under the dinitrogen cold stream on the diffractometer. The low-temperature accessory for the diffractometer is a locally modified Syntex LT-1 system. Final lattice constants are summarized in Table I. Complete crystallographic details are given in Table SIII of the supplementary material. Final cell constants are from the least-squares refinement of 25 automatically centered reflections with $24 < 2\theta < 30°$. Initial intensity data reduction utilized the 25% scan extensions for estimations of background that are standard with Nonius diffractometer software. The data from this initial data reduction was used for structure solution and refinement. Data having $F_o > 3\sigma(F_o)$ were considered observed and used in the structure analysis. There were a total of 7005 data for the form 1 analysis and 4257 data for the form 2 analysis. Shortly after completion of these structure determinations, the profile analysis software of R. H. Blessing[13] of the Medical Foundation of Buffalo became available for our use. We took this opportunity to compare data reduced with these routines with our previous data reduction procedures. The Blessing data reduction algorithms produced clearly superior data sets. The number of observed data (7720 and 4748) at the same σ level is thus increased by about 10%, clearly indicating the improvement in signal to noise levels resulting rom individualized peak profile and background analysis.

Table I. Crystal Data for [Zn(TPP)$OClO_3$]·$2CH_2Cl_2$

	form 1	form 2
formula	$ZnCl_5O_4N_4C_{46}H_{32}$	
fw, amu	947.43	
space group	$P2_1/c$	$P2_1/n$
temp, K	118	118
a, Å	13.503 (4)	12.485 (3)
b, Å	18.582 (5)	17.141 (11)
c, Å	17.236 (8)	19.443 (5)
β, deg	109.32 (3)	95.29 (2)
V, Å^3	4081.2	4143.2
Z	4	4
radiation	graphite-monochromated Mo Kα (0.710 73 Å)	
μ(Mo Kα), mm^{-1}	0.995	0.980
R_1	0.058	0.061
R_2	0.061	0.063

The structures of both crystalline phases were solved by using the direct-methods program MULTAN78.[14] All atoms, including those of the solvate molecules, appear to be completely ordered. During the course of the full-matrix least-squares refinement, difference Fourier syntheses indicated electron density maxima corresponding to reasonable positions of all hydrogen atom positions in the porphyrin ligand and the solvate molecules. Tentative hydrogen atom positions were included in subsequent cycles of least-squares refinement. Given the apparent quality of the data, due to both the low-temperature data collection and the Blessing profile analysis, atomic coordinates and temperature factors of the hydrogen atoms were included as variables in the calculations. Three temperature factors (in form 2) did not remain positive definite and were held at fixed values. Otherwise, all hydrogen atom parameters were quite reasonable and are reported here along with the analogous parameters for the other atoms of the structure. Refinement was carried to con-

(10) Adler, A. D.; Longo, F. R.; Finarelli, J. D.; Goldamacher, J.; Assour, I.; Korsakoff, L. *J. Org. Chem.* **1967**, *32*, 476.

(11) Bleaney, B.; Bowers, K. D. *Proc. R. Soc. London* **1952**, *A214*, 451.

(12) In the earliest stages of this investigation, we attempted to determine the structure of crystals of what were most probably that of form 2 at room temperature. We used crystals that had been allowed to stand, after isolation, at room temperature for about 3 months before data collection could be commenced. This structural analysis has not been finished owing to our inability to adequately model the two disordered and partially occupied dichloromethane solvate molecules. Crystal data: a = 13.301 Å, b = 16.863 Å, c = 19.667 Å, and β = 98.42°. Although the cell constants may appear different enough from that of Form 2 to raise questions about the isomorphism, use of the room-temperature coordinates and low-temperature intensity data leads to least-squares convergence and essential equivalence with the independently obtained low-temperature coordinates, thus confirming essential isomorphism of the two species.

(13) Blessing, R. H. *Crystallogr. Rev.* **1987**, *1*, 3–58.

(14) Programs used in this study included local modifications of Main, Hull, Lessinger, Germain, Declerq, and Woolfson's MULTAN78, Jacobson's ALLS, Zalkin's FORDAP, Busing and Levy's ORFFE and ORFLS, and Johnson's ORTEP2. Atomic form factors were from: Cromer, D. T.; Mann, J. B. *Acta Crystallogr., Sect. A* **1968**, *A24*, 321–323. Real and imaginary corrections for anomalous dispersion in the form factor of the zinc and chlorine atoms were from: Cromer, D. T.; Liberman, D. J. *J. Chem. Phys.* **1970**, *53*, 1891–1898. Scattering factors for hydrogen were from: Stewart, R. F.; Davidson, E. R.; Simpson, W. T. *Ibid.* **1965**, *42*, 3175–3187. All calculations were performed on a VAX 11/730 computer.

Table II. Fractional Coordinates for $[Zn(TPP)OClO_4]\cdot 2CH_2Cl_2$ (Form 1)[a]

atom	x	y	z	atom	x	y	z
Zn(1)	0.174362 (29)	0.005113 (20)	0.124385 (23)	C(13)	−0.15182 (26)	−0.10749 (19)	0.12885 (22)
Cl(1)	0.32537 (7)	−0.03081 (5)	0.30993 (5)	C(14)	−0.17572 (29)	−0.08409 (20)	0.19769 (23)
Cl(2)	0.16610 (9)	0.16162 (6)	0.34450 (8)	C(15)	−0.2599 (3)	−0.11342 (24)	0.21627 (26)
Cl(3)	−0.02108 (10)	0.09197 (7)	0.35887 (9)	C(16)	−0.3202 (3)	−0.16635 (25)	0.16674 (28)
Cl(4)	0.22735 (14)	0.47601 (14)	0.06697 (11)	C(17)	−0.29823 (29)	−0.18953 (22)	0.09788 (26)
Cl(5)	0.38203 (25)	0.36429 (11)	0.08067 (19)	C(18)	−0.21409 (28)	−0.16005 (20)	0.07868 (22)
O(1)	0.22452 (19)	−0.00270 (17)	0.25489 (15)	C(19)	0.32266 (27)	−0.22997 (18)	0.08797 (21)
O(2)	0.40906 (24)	0.00955 (22)	0.29839 (19)	C(20)	0.27802 (28)	−0.27853 (20)	0.02481 (22)
O(3)	0.32373 (26)	−0.02194 (18)	0.39274 (16)	C(21)	0.3309 (3)	−0.34091 (20)	0.01774 (23)
O(4)	0.3321 (3)	−0.10496 (18)	0.29144 (2)	C(22)	0.4278 (3)	−0.35578 (20)	0.07482 (24)
N(1)	0.30841 (22)	−0.02901 (16)	0.10560 (17)	C(23)	0.47049 (29)	−0.30996 (21)	0.14100 (24)
N(2)	0.21985 (22)	0.11069 (15)	0.11623 (17)	C(24)	0.41907 (28)	−0.24696 (19)	0.14717 (22)
N(3)	0.02713 (22)	0.04232 (15)	0.11412 (17)	C(25)	0.0996 (3)	0.08033 (23)	0.3413 (3)
N(4)	0.11332 (21)	−0.09756 (15)	0.09812 (16)	C(26)	0.3567 (5)	0.4556 (3)	0.0691 (3)
C(a1)	0.33273 (26)	−0.09821 (18)	0.08971 (20)	H(b1)	0.464 (4)	−0.1406 (26)	0.0620 (28)
C(a2)	0.39256 (25)	0.01230 (18)	0.10704 (20)	H(b2)	0.531 (4)	−0.0122 (29)	0.083 (3)
C(a3)	0.32343 (27)	0.13141 (19)	0.13350 (21)	H(b3)	0.398 (5)	0.229 (3)	0.176 (3)
C(a4)	0.16743 (26)	0.17042 (17)	0.12699 (21)	H(b4)	0.214 (4)	0.2782 (29)	0.164 (3)
C(a5)	−0.00595 (26)	0.11294 (19)	0.10985 (21)	H(b5)	−0.1563 (29)	0.1552 (21)	0.0907 (22)
C(a6)	−0.05889 (23)	0.00132 (20)	0.10800 (18)	H(b6)	−0.208 (4)	0.0302 (26)	0.0918 (28)
C(a7)	0.02100 (27)	−0.12065 (18)	0.10777 (20)	H(b7)	−0.033 (4)	−0.2245 (26)	0.1234 (28)
C(a8)	0.17033 (26)	−0.15838 (18)	0.09830 (20)	H(b8)	0.135 (3)	−0.2671 (24)	0.1102 (25)
C(b1)	0.43192 (26)	−0.09830 (19)	0.07474 (21)	H(2)	0.486 (4)	0.2028 (24)	0.0752 (28)
C(b2)	0.46962 (27)	−0.03018 (19)	0.08656 (21)	H(3)	−0.351 (4)	0.2501 (28)	0.118 (3)
C(b3)	0.33453 (28)	0.20601 (20)	0.15710 (22)	H(4)	−0.220 (4)	0.1923 (27)	0.230 (3)
C(b4)	0.23822 (28)	0.23032 (20)	0.15165 (22)	H(5)	−0.257 (4)	0.0882 (26)	0.2843 (29)
C(b5)	−0.11717 (26)	0.11490 (19)	0.09843 (20)	H(6)	0.583 (4)	0.0439 (28)	0.2387 (29)
C(b6)	−0.14906 (26)	0.04560 (19)	0.09787 (21)	H(8)	0.059 (4)	0.2953 (27)	0.033 (3)
C(b7)	0.02160 (28)	−0.19846 (19)	0.11393 (21)	H(9)	−0.014 (4)	0.406 (3)	0.038 (3)
C(b8)	0.11364 (27)	−0.22126 (18)	0.10763 (21)	H(10)	−0.101 (3)	0.4214 (23)	0.1299 (23)
C(m1)	0.40463 (26)	0.08638 (19)	0.12830 (20)	H(11)	−0.122 (4)	0.3288 (26)	0.2172 (29)
C(m2)	0.05870 (26)	0.17378 (18)	0.11903 (20)	H(12)	−0.044 (3)	0.2218 (25)	0.2165 (27)
C(m3)	−0.05929 (26)	−0.07518 (18)	0.11242 (20)	H(14)	−0.136 (4)	−0.0514 (27)	0.232 (3)
C(m4)	0.27303 (25)	−0.15891 (19)	0.09166 (20)	H(15)	−0.280 (5)	−0.099 (3)	0.261 (4)
C(1)	0.51248 (27)	0.11642 (19)	0.15161 (21)	H(16)	−0.380 (4)	−0.184 (3)	0.180 (3)
C(2)	0.5350 (3)	0.17961 (21)	0.11683 (23)	H(17)	−0.342 (5)	−0.220 (3)	0.063 (3)
C(3)	0.6360 (3)	0.20908 (23)	0.14593 (27)	H(18)	−0.204 (4)	−0.1726 (26)	0.034 (3)
C(4)	0.7129 (3)	0.17558 (26)	0.20861 (28)	H(20)	0.215 (4)	−0.2687 (27)	−0.013 (3)
C(5)	0.6923 (3)	0.11215 (26)	0.24196 (26)	H(21)	0.299 (4)	−0.3705 (28)	−0.021 (3)
C(6)	0.59243 (28)	0.08276 (21)	0.21372 (23)	H(22)	0.461 (4)	−0.401 (3)	0.066 (3)
C(7)	0.01347 (26)	0.24570 (18)	0.12318 (21)	H(23)	0.533 (5)	−0.319 (3)	0.177 (4)
C(8)	0.02397 (28)	0.30207 (19)	0.07255 (23)	H(24)	0.450 (4)	−0.2151 (27)	0.187 (3)
C(9)	−0.0205 (3)	0.36850 (20)	0.07571 (25)	H(25a)	0.148 (5)	0.050 (3)	0.387 (4)
C(10)	−0.0772 (3)	0.37988 (20)	0.12907 (25)	H(25b)	0.092 (6)	0.057 (4)	0.296 (5)
C(11)	−0.08703 (29)	0.32557 (21)	0.18068 (23)	H(26a)	0.405 (5)	0.478 (3)	0.120 (4)
C(12)	−0.04180 (28)	0.25876 (19)	0.17852 (22)	H(26b)	0.361 (5)	0.467 (4)	0.014 (4)

[a] The estimated standard deviations of the least significant digits are given in parentheses.

vergence, leading to the final values of the discrepancy indices listed in Table I, where

$$R_1 = \sum||F_o| - |F_c||/\sum|F_o|$$

$$R_2 = [\sum w(|F_o| - |F_c|)^2/\sum w(F_o)^2]^{1/2}$$

Final difference Fourier syntheses were judged to be featureless with the largest peak (in either structure) having a value of 0.70 e/Å^3. All large peaks were located near either a zinc or a chlorine atom. Previously completed refinements utilizing the intensity data reduced by the standard Nonius background estimation method gave R values were significantly higher than those of Table I, especially after noting the approximate 10% increase in the number of "observed" reflections (utilizing the same observation criterion), and indicate the appropriateness and improvements of the Blessing data reduction algorithms.[15] Final values of atomic coordinates are reported in Tables II (form 1) and III (form 2), and those of the anisotropic temperature factors and isotropic hydrogen atom thermal parameters are given in Tables SIV and SV. All final values are based on the parameters from the least-squares refinements utilizing the profile analysis data.

Results and Discussion

Crystallization Experiments. During the course of our crystallization experiments with $[Zn(TPP^{\bullet})(OClO_3)]$, we have apparently isolated at least eight different crystalline phases of this compound, including the previously reported β phase of Spaulding et al.[9] All phases were obtained from dichloromethane solution. Crystal phase identification was accomplished by single-crystal X-ray examination as well as by microscopic examination. During the course of the identifications, approximately 35 crystals were subjected to cell constant determination by single-crystal diffractometry. Two crystalline phases (form 1 and the β phase) are readily recognizable and distinguishable from all other phases while the remaining several phases are much less so. The morphology of form 1 is best described as six-sided monoclinic rhombs with either nearly equal dimensions or with only one direction elongated. The β-phase crystals were always found to be rectangular needles with dimensional ratios of approximately 6:2:1. Forms 2 and 3 are not easily distinguishable from each other. Their morphology is that of monoclinic rhombs with one small dimension (i.e. platelike); frequently these crystals had additional faces. Crystals of form 4 were chunky prisms readily distinguished from the β phase but not necessarily from other cocrystallized phases. Phase assignments made by optical methods were confirmed by X-ray examination in a number of cases. For form 1 and the β phase our optical assignments always turned out to be correct.

The first two phases that we were able to prepare were made by method A. We have designated these as forms 1 and 2. Both were isolated as bis(dichloromethane) solvates and have been

(15) The refinements using the standard Nonius background estimation method gave R_1 = 0.058 (0.058) and R_2 = 0.069 (0.064) for form 1 (form 2).

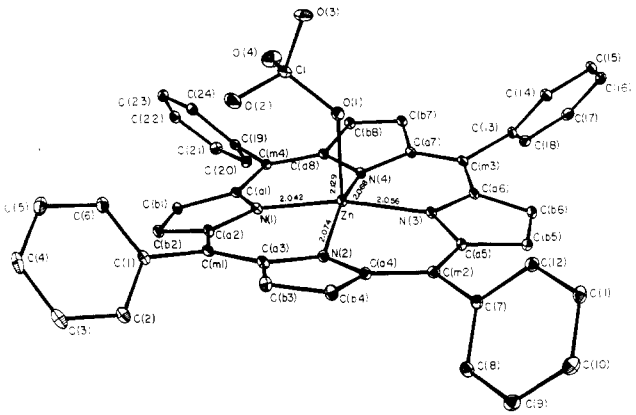

Figure 1. ORTEP diagram of an isolated $[Zn(TPP^{\bullet})(OClO_3)]$ molecule (form 1) as it exists in the crystal. Illustrated in the diagram are the atom-labeling scheme and the values of the bond distances in the coordination group. Thermal ellipsoids are contoured at the 75% level. The extreme nonplanar nature of the porphyrin core is evident in the drawing.

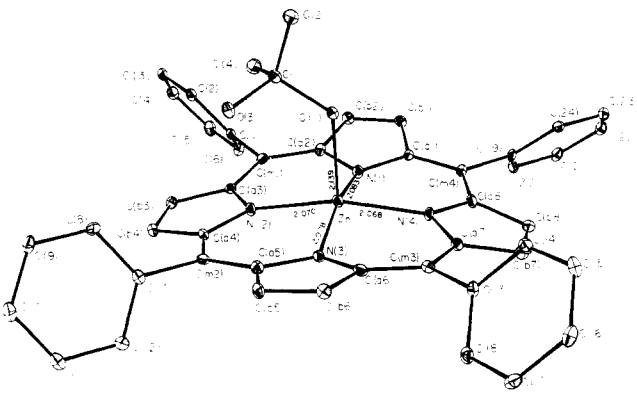

Figure 2. ORTEP diagram of an isolated molecule of form 2. The orientation of the molecule has been chosen to be similar to that illustrated in Figure 1. All information appropriate for Figure 1 also pertains here.

characterized by complete structure determinations. Our initial results led us to believe that temperature was the significant controlling factor with form 1 isolated from the experiments performed at room temperature and form 2 from crystallization at −15 °C. Subsequent experiments lead us to conclude that these preferences were only tendencies. The form 1 phase is always present in method A crystallizations and probably the form 2 phase is always present as well. In addition, during the several subsequent experiments, we identified the presence of two additional crystalline phases: a new phase we designate as form 3[16] as well as small amounts of the known β phase.

The second crystallizations procedure (method B) was found to be useful in preparing adequate amounts of the β phase for magnetic susceptibility measurements. Crystallization results by this method apparently gave several different phases: the β phase and a complex mixture of species we designate as forms 4–7.[17] The relative amounts of these phases were clearly dependent on temperature. The approximate β:forms 4–7 ratios found were 6.6:1 (40 °C), 1:3.4 (30 °C), and 1:5.2 (25 °C). Estimates of the relative amounts were made by physically dividing the sample

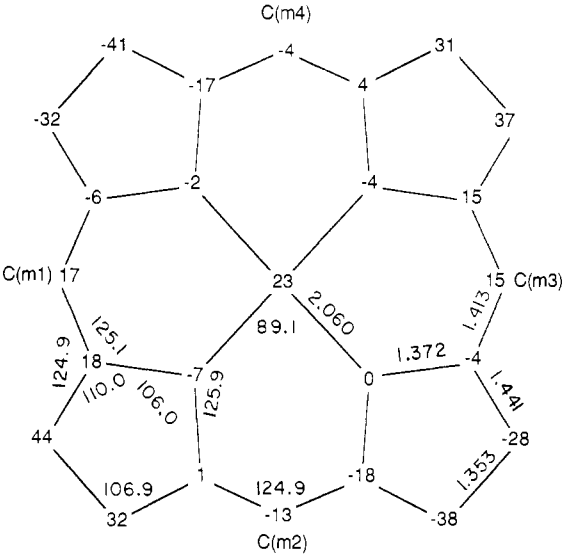

Form 1

Figure 3. Formal diagram of the porphinato core of the $[Zn(TPP^{\bullet})(OClO_3)]$ molecule (form 1) displaying the perpendicular displacement of the atoms from the mean plane of 24-atom core. Shown at each atom position of the core is the displacement of that atom, in units of 0.01 Å, from the best least-squares plane. Also entered onto the diagram are the averaged values of the various chemical types of bond distances and bond angles in the core.

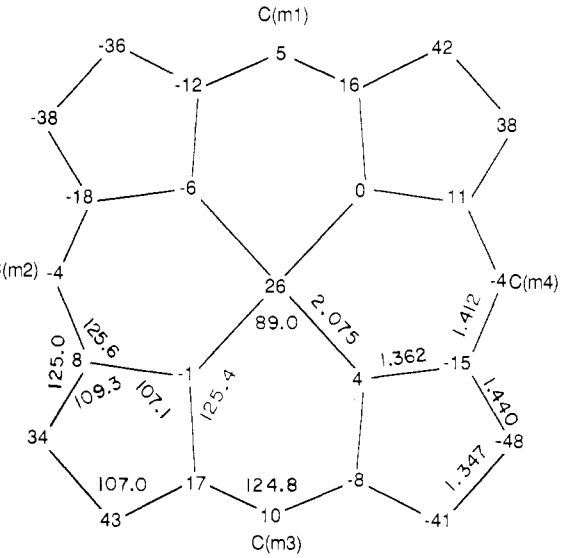

Form 2

Figure 4. Equivalent information given in Figure 3 displayed here for the molecule in crystalline form 2.

into two parts under microscopic examination and weighing. It is not clear whether all of these additional phases are present in each crystallization experiment. At no time did we observe the additional phase (α) previously reported by Spaulding et al.[9] This is presumably the result of using experimental crystallization conditions that are quite different from those utilized by Spaulding et al.[9] They utilized electrochemical rather than chemical procedures to oxidize neutral Zn(TPP) to the radical. This necessitates the presence of large amounts of supporting electrolyte ($Pr_4N^+ClO_4^-$) not present under our conditions although the dichloromethane solvent was common to both preparative procedures. The idea behind our choice of a chemical oxidation procedure was the potential advantage of being able to obtain adequate samples for susceptibility measurements that were free from the contamination of cocrystallized supporting electrolyte. Nevertheless, for a different reason, considerable labor of hand

(16) Crystal data for form 3: triclinic, a = 13.91 Å, b = 15.15 Å, c = 18.85 Å, α = 93.21°, β = 94.11°, γ = 102.27°, V = 3864 Å^3.

(17) In this context, forms 4–7 designate species known to be present as well as other possible phases including the possibility of an unassigned β phase. Crystal data for known species are given as follows. Form 4: triclinic, a = 11.16 Å, b = 11.60 Å, c = 16.57 Å, α = 75.43°, β = 76.95°, γ = 73.52°, V = 1963 Å^3. Form 5: triclinic, a = 13.50 Å, b = 26.37 Å, c = 13.45 Å, α = 84.90°, β = 53.04°, γ = 93.25°, V = 3774 Å. Form 6: monoclinic, a = 14.00 Å, b = 17.35 Å, c = 15.37 Å, β = 102.72°, V = 3641 Å^3. Form 7: triclinic, a = 17.81 Å, b = 36.43 Å, c = 13.71 Å, α = 97.26°, β = 112.28°, γ = 76.67°, V = 7997 Å^3. Delauney reductions on all forms did not reveal any hidden symmetry. Axial photographs confirmed axial lengths and symmetry conditions.

Table III. Fractional Coordinates for $[Zn(TPP)OClO_4]\cdot 2CH_2Cl_2$ (Form 2)[a]

atom	x	y	z	atom	x	y	z
Zn(1)	0.96279 (6)	0.15301 (4)	0.53712 (4)	C(13)	0.7357 (5)	−0.0743 (4)	0.5740 (3)
Cl(1)	0.84507 (13)	0.29333 (9)	0.60952 (8)	C(14)	0.7223 (5)	−0.0932 (4)	0.6428 (3)
Cl(2)	−0.01865 (17)	0.08208 (13)	0.12863 (11)	C(15)	0.6564 (5)	−0.1531 (4)	0.6591 (3)
Cl(3)	0.00030 (18)	0.20316 (13)	0.23476 (11)	C(16)	0.6030 (5)	−0.1966 (4)	0.6076 (4)
Cl(4)	0.14541 (20)	0.37677 (14)	0.15533 (12)	C(17)	0.6134 (5)	−0.1788 (4)	0.5389 (4)
Cl(5)	0.25334 (25)	0.43206 (15)	0.28641 (14)	C(18)	0.6793 (5)	−0.1186 (4)	0.5229 (3)
O(1)	0.8875 (4)	0.21341 (26)	0.61599 (22)	C(19)	1.2533 (5)	0.0389 (3)	0.6990 (3)
O(2)	0.8018 (4)	0.3108 (3)	0.67341 (25)	C(20)	1.3615 (5)	0.0380 (4)	0.6871 (3)
O(3)	0.7623 (4)	0.29702 (29)	0.55348 (24)	C(21)	1.4378 (6)	0.0051 (4)	0.7342 (4)
O(4)	0.9309 (4)	0.3445 (3)	0.59899 (25)	C(22)	1.4087 (6)	−0.0251 (4)	0.7951 (4)
N(1)	1.1221 (4)	0.1813 (3)	0.56824 (28)	C(23)	1.3022 (7)	−0.0240 (4)	0.8085 (4)
N(2)	0.9596 (4)	0.2405 (3)	0.46359 (26)	C(24)	1.2244 (5)	0.0079 (4)	0.7615 (3)
N(3)	0.8223 (4)	0.10756 (29)	0.48708 (25)	C(25)	0.0633 (7)	0.1258 (7)	0.1947 (6)
N(4)	0.9847 (4)	0.04933 (29)	0.59101 (27)	C(26)	0.2083 (9)	0.3509 (6)	0.2372 (6)
C(a1)	1.1845 (5)	0.1470 (4)	0.6210 (3)	H(b1)	1.313 (7)	0.192 (5)	0.672 (4)
C(a2)	1.1673 (5)	0.2519 (4)	0.5569 (3)	H(b2)	1.292 (5)	0.304 (4)	0.606 (3)
C(a3)	1.0365 (5)	0.2962 (3)	0.4588 (3)	H(b3)	1.056 (5)	0.382 (4)	0.387 (3)
C(a4)	0.8792 (5)	0.2556 (4)	0.4138 (3)	H(b4)	0.870 (5)	0.344 (4)	0.344 (3)
C(a5)	0.7532 (5)	0.1490 (4)	0.4416 (3)	H(b5)	0.599 (5)	0.128 (4)	0.416 (3)
C(a6)	0.7653 (5)	0.0480 (4)	0.5108 (3)	H(b6)	0.596 (6)	0.020 (4)	0.495 (3)
C(a7)	0.9138 (5)	−0.0106 (4)	0.5886 (3)	H(b7)	0.935 (6)	−0.121 (5)	0.624 (4)
C(a8)	1.0766 (5)	0.0253 (4)	0.6300 (3)	H(b8)	1.120 (5)	−0.085 (4)	0.673 (3)
C(b1)	1.2708 (6)	0.1992 (4)	0.6450 (4)	H(2)	1.075 (5)	0.451 (4)	0.522 (3)
C(b2)	1.2594 (5)	0.2634 (4)	0.6058 (3)	H(3)	1.163 (6)	0.570 (4)	0.503 (4)
C(b3)	1.0048 (5)	0.3463 (4)	0.4008 (3)	H(4)	1.334 (6)	0.561 (4)	0.476 (4)
C(b4)	0.9072 (6)	0.3219 (4)	0.3737 (4)	H(5)	1.424 (6)	0.445 (4)	0.454 (4)
C(b5)	0.6497 (6)	0.1131 (4)	0.4374 (4)	H(6)	1.326 (5)	0.335 (4)	0.473 (3)
C(b6)	0.6548 (5)	0.0519 (4)	0.4807 (3)	H(8)	0.674 (4)	0.352 (4)	0.409 (3)
C(b7)	0.9632 (5)	−0.0766 (4)	0.6245 (3)	H(9)	0.539 (5)	0.399 (4)	0.333 (3)
C(b8)	1.0644 (5)	−0.0554 (4)	0.6493 (3)	H(10)	0.474 (6)	0.327 (4)	0.239 (4)
C(m1)	1.1309 (5)	0.3051 (4)	0.5040 (3)	H(11)	0.554 (6)	0.214 (4)	0.208 (4)
C(m2)	0.7793 (5)	0.2157 (4)	0.4055 (3)	H(12)	0.684 (6)	0.170 (4)	0.291 (3)
C(m3)	0.8066 (5)	−0.0103 (4)	0.5567 (3)	H(14)	0.753 (5)	−0.052 (4)	0.678 (4)
C(m4)	1.1686 (5)	0.0721 (4)	0.6475 (3)	H(15)	0.639 (6)	−0.157 (5)	0.697 (4)
C(1)	1.1917 (5)	0.3786 (4)	0.4975 (3)	H(16)	0.566 (6)	−0.229 (5)	0.618 (4)
C(2)	1.1412 (5)	0.4496 (4)	0.5084 (3)	H(17)	0.578 (4)	−0.207 (3)	0.509 (3)
C(3)	1.1961 (6)	0.5192 (4)	0.5003 (3)	H(18)	0.694 (4)	−0.119 (3)	0.482 (3)
C(4)	1.2994 (6)	0.5181 (4)	0.4806 (4)	H(20)	1.380 (5)	0.054 (4)	0.644 (4)
C(5)	1.3498 (6)	0.4484 (4)	0.4710 (4)	H(21)	1.502 (5)	0.007 (3)	0.7260 (28)
C(6)	1.2963 (5)	0.3789 (4)	0.4791 (4)	H(22)	1.465 (6)	−0.049 (5)	0.829 (4)
C(7)	0.6930 (5)	0.2507 (4)	0.3561 (3)	H(23)	1.275 (5)	−0.041 (4)	0.843 (3)
C(8)	0.6489 (6)	0.3217 (4)	0.3704 (4)	H(24)	1.159 (6)	0.011 (4)	0.776 (4)
C(9)	0.5669 (5)	0.3530 (4)	0.3254 (4)	H(25a)	0.113 (10)	0.141 (8)	0.170 (6)
C(10)	0.5316 (6)	0.3146 (4)	0.2657 (4)	H(25b)	0.068 (29)	0.200 (24)	0.191 (19)
C(11)	0.5748 (6)	0.2433 (4)	0.2509 (4)	H(26a)	0.287 (9)	0.319 (7)	0.223 (6)
C(12)	0.6549 (5)	0.2106 (4)	0.2958 (3)	H(26b)	0.180 (10)	0.309 (8)	0.256 (7)

[a] The estimated standard deviations of the least significant digits are given in parentheses.

sorting of crystals was still required for the susceptibility samples.

The particular phase of $[Zn(TPP^{\bullet})(OClO_3)]$ prepared is clearly dependent on experimental conditions including the temperature and rate of diffusion of the nonsolvent hexane into the dichloromethane solution. Unfortunately, we are unable, despite significant effort, to state definitive recipes for the preparation of a particular *pure* phase.

Structural Analyses. The molecular structure of an isolated molecule of form 1 of $[Zn(TPP^{\bullet})(OClO_3)]$ is illustrated in Figure 1, and that for form 2 is shown in Figure 2. The close similarity of the molecular features of the two crystalline forms is evident. The molecular structure similarity of these two crystalline forms with that shown by the β phase described by Spaulding et al.[9] is striking. Equally striking is the similarity of the porphinato core conformation in the three phases.

Formal diagrams of the porphinato cores in the two crystalline forms of the molecule are given in Figures 3 and 4. We display in these two diagrams the perpendicular displacement of each atom from the mean plane of the 24-atom core. As is readily observed from the diagrams, the pyrrole rings are displaced, alternatively, above and below the mean plane of the porphinato core. The approximate D_{2d}-type ruffled geometry of these species differs from the more usual D_{2d}-type ruffled core by a 45° rotation of the point group symmetry operators around the major 2-fold axis that is perpendicular to the porphyrin plane. Both complex species have the same type of D_{2d}-ruffled geometry that Scheidt and Lee[8] showed was found for all π-cation-radical metalloporphyrin complexes known at the time of their review. The review traced the origin of this unusual saddle-shaped conformation to the steric requirements of face-to-face dimer formation. Solid-state dimer formation is also exhibited by both forms of $[Zn(TPP^{\bullet})(OClO_3)]$. An edge-on view of the pair of porphyrin molecules of form 1 is shown in Figure 5; an equivalent drawing for form 2 is given in the supplementary material as Figure S1.

Such saddle-shaped conformations are required to allow the phenyl rings to be more nearly coplanar with the porphinato core, a necessity if the two 24-atom porphinato cores of tetraphenylporphyrin derivatives are to overlap to a substantial degree. Scheidt and Lee[8] noted that the values for the dihedral angles between the phenyl group planes and the mean porphinato core in dimer structures tend to be significantly smaller than normal.[18] Such is the case here as well. The dihedral angles are tabulated (Table VI) for all three crystalline forms of $[Zn(TPP^{\bullet})(OClO_3)]$ along with three parameters used previously[8] to succinctly summarize the quantitative ruffling of the core.[19]

(18) Normal values range from 60 up to 90°.

(19) Reference 8 should be consulted for complete tabulations of core conformations for the π-cation radicals, all of which are tetraphenylporphyrin species. This reference also tabulates a number of other numerical descriptors of the various radical species that are used in this paper.

Table IV. Bond Distances (Å) for $[Zn(TPP)OClO_3]\cdot 2CH_2Cl_2$

	form 1	form 2		form 1	form 2
Zn-Zn	5.220 (4)	5.542 (4)	Zn-O(1)	2.129 (3)	2.139 (4)
Zn-N(1)	2.042 (3)	2.083 (5)	Cl(2)-C(25)	1.749 (4)	1.737 (10)
Zn-N(2)	2.074 (3)	2.070 (5)	Cl(3)-C(25)	1.766 (4)	1.761 (11)
Zn-N(3)	2.056 (3)	2.078 (5)	Cl(4)-C(26)	1.776 (6)	1.766 (11)
Zn-N(4)	2.068 (3)	2.068 (5)	Cl(5)-C(26)	1.729 (6)	1.751 (10)
Cl(1)-O(1)	1.474 (3)	1.470 (5)	N(1)-C(a1)	1.377 (4)	1.363 (8)
Cl(1)-O(2)	1.424 (3)	1.432 (5)	N(1)-C(a2)	1.365 (4)	1.361 (8)
Cl(1)-O(3)	1.444 (3)	1.432 (5)	N(2)-C(a3)	1.385 (4)	1.364 (8)
Cl(1)-O(4)	1.424 (3)	1.414 (5)	N(2)-C(a4)	1.362 (4)	1.353 (8)
N(3)-C(a5)	1.380 (4)	1.376 (8)	N(4)-C(a7)	1.380 (4)	1.355 (8)
N(3)-C(a6)	1.364 (4)	1.349 (8)	N(4)-C(a8)	1.367 (4)	1.378 (8)
C(a1)-C(b1)	1.445 (4)	1.444 (9)	C(a2)-C(b2)	1.440 (4)	1.436 (9)
C(a1)-C(m4)	1.393 (5)	1.404 (9)	C(a2)-C(m1)	1.420 (5)	1.419 (9)
C(a3)-C(b3)	1.438 (5)	1.443 (9)	C(a4)-C(m2)	1.430 (5)	1.419 (9)
C(a3)-C(m1)	1.406 (5)	1.412 (9)	C(a4)-C(b4)	1.437 (5)	1.440 (9)
C(a5)-C(b5)	1.449 (5)	1.427 (10)	C(a6)-C(b6)	1.431 (5)	1.450 (9)
C(a5)-C(m2)	1.405 (5)	1.395 (9)	C(a6)-C(m3)	1.424 (5)	1.405 (9)
C(a7)-C(b7)	1.449 (5)	1.437 (9)	C(a8)-C(b8)	1.435 (5)	1.445 (9)
C(a7)-C(m3)	1.398 (5)	1.422 (9)	C(a8)-C(m4)	1.429 (4)	1.416 (9)
C(b1)-C(b2)	1.354 (5)	1.339 (10)	C(b3)-C(b4)	1.350 (5)	1.348 (10)
C(b5)-C(b6)	1.357 (5)	1.343 (10)	C(b7)-C(b8)	1.351 (5)	1.359 (9)
C(m1)-C(1)	1.486 (5)	1.482 (9)	C(m2)-C(7)	1.481 (5)	1.501 (9)
C(m3)-C(13)	1.495 (5)	1.469 (9)	C(m4)-C(19)	1.492 (5)	1.499 (8)
C(1)-C(2)	1.397 (5)	1.395 (9)	C(2)-C(3)	1.400 (6)	1.391 (10)
C(1)-C(6)	1.392 (5)	1.386 (9)	C(3)-C(4)	1.375 (7)	1.379 (10)
C(4)-C(5)	1.380 (7)	1.371 (10)	C(5)-C(6)	1.385 (6)	1.381 (10)
C(7)-C(8)	1.400 (5)	1.374 (9)	C(8)-C(9)	1.382 (5)	1.393 (9)
C(7)-C(12)	1.413 (5)	1.404 (9)	C(9)-C(10)	1.393 (6)	1.371 (10)
C(10)-C(11)	1.380 (6)	1.376 (11)	C(11)-C(12)	1.390 (5)	1.384 (10)
C(13)-C(14)	1.398 (5)	1.402 (9)	C(14)-C(15)	1.390 (5)	1.371 (10)
C(13)-C(18)	1.388 (5)	1.389 (10)	C(15)-C(16)	1.378 (7)	1.371 (10)
C(16)-C(17)	1.384 (6)	1.387 (10)	C(17)-C(18)	1.396 (5)	1.372 (10)
C(19)-C(20)	1.389 (5)	1.392 (9)	C(20)-C(21)	1.388 (5)	1.379 (10)
C(19)-C(24)	1.399 (5)	1.403 (9)	C(21)-C(22)	1.380 (6)	1.372 (11)
C(22)-C(23)	1.387 (6)	1.377 (11)	C(23)-C(24)	1.383 (5)	1.384 (10)

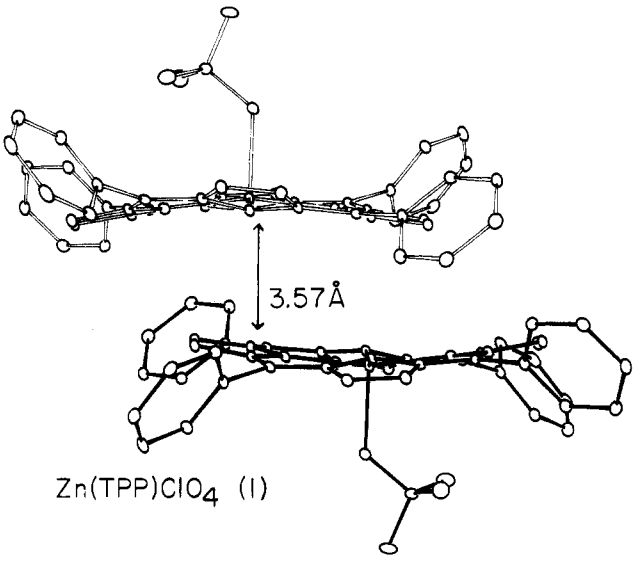

Figure 5. Edge-on view of the dimer in form 1 of $[Zn(TPP^{\bullet})(OClO_3)]$. The ruffling that allows the phenyl groups to be more nearly coplanar with the core can be seen in this diagram.

Although all three species are dimeric in the solid state, there are interesting detailed differences in the interactions. Both new forms are more tightly coupled than the β phase. The degree of interaction and overlap between the two cores can be expressed in terms of the mean plane separation, the Ct···Ct separation, and the lateral shift of the two rings.[20] Values for these parameters are listed in Table VI, and the progression, measured in terms of either of the two independent variables, is evident. We have previously[8] defined a more precise geometrical description to define the relative orientations of the two macrocyclic rings. In this description, two vectors, **u** and **v**, are defined by the opposite pairs of nitrogen atoms of the tetrapyrrole. The two vectors are then used to define the orthogonal coordinate system x, y, z where

$$x = \mathbf{u} \qquad y = (\mathbf{u} \times \mathbf{v}) \times \mathbf{u} \qquad z = (\mathbf{u} \times \mathbf{v})$$

With this definition, axes x and y are approximately in the plane of the macrocycle and z is approximately perpendicular to the mean plane of the ring. This new orthogonal coordinate system is used to define the position of the center (Ct) of the adjacent molecule in the dimer. In our calculations we have required the x direction to correspond to the N···N direction that is effectively eclipsed by the Zn–O–Cl plane. These results are given in Table VI and schematically depicted in the composite overlap diagram of Figure 6.[21] The significant variation in the overlap of the paired cores in the three phases is evident. In terms of the categories suggested by Scheidt and Lee,[8] Forms 1 and 2 are described as having an intermediate interaction, while the β phase would be classed a member of the weak interaction group. Implicit in the diagram of Figure 6 is the fact that the two molecules of the dimer in each phase are related to each other by a crystallographic inversion center. This leads to the requirement that the equivalent N···N axes in the two molecules of the dimer will be parallel. This crystallographically required symmetry element also leads to the fact that each pair of molecular planes are precisely parallel.

The varying strength of the intermolecular interactions appears to lead to variations in the coordination group geometry: both the displacement of the zinc ion out of the porphyrin plane and the axial Zn–O bond length are affected. As shown in Table VI, increased ring overlap (smaller lateral shift and presumably a

(20) The mean plane separation is the average perpendicular distance of the atoms of one core from the mean plane of the other core. Ct is the defined as the center of the ring and the lateral shift is the relative displacement of the two ring centers in the plane of one core. Specification of any two of these parameters automatically defines the third.

(21) For comparison purposes, individual paired overlap diagrams similar to that in Figure 6 are included as supplementary material.

Table V. Bond Angles (deg) for $[Zn(TPP)OClO_3]\cdot 2CH_2Cl_2$

	form 1	form 2		form 1	form 2
O(1)ZnN(1)	99.1 (1)	98.6 (2)	N(2)C(a3)C(b3)	109.4 (3)	109.0 (5)
O(1)ZnN(2)	97.9 (1)	99.3 (2)	N(2)C(a3)C(m1)	125.1 (3)	125.9 (6)
O(1)ZnN(3)	94.3 (1)	96.3 (2)	C(m1)C(a3)C(b3)	125.5 (3)	125.1 (6)
O(1)ZnN(4)	97.6 (1)	95.7 (2)	N(2)C(a4)C(b4)	110.3 (3)	109.7 (6)
N(1)ZnN(2)	89.1 (1)	89.4 (2)	N(2)C(a4)C(m2)	125.9 (3)	125.2 (6)
N(1)ZnN(3)	166.7 (1)	165.1 (2)	C(m2)C(a4)C(b4)	123.8 (3)	125.0 (6)
N(4)ZnN(4)	89.4 (1)	88.5 (2)	N(3)C(a5)C(b5)	109.5 (3)	108.9 (6)
N(2)ZnN(3)	88.6 (1)	89.2 (2)	N(3)C(a5)C(m2)	125.5 (3)	125.8 (6)
N(2)ZnN(4)	164.4 (1)	165.0 (2)	C(m2)C(a5)C(b5)	124.9 (3)	125.3 (6)
N(3)ZnN(4)	89.3 (1)	89.0 (2)	N(3)C(a6)C(b6)	110.9 (3)	109.8 (6)
O(1)Cl(1)O(2)	109.3 (2)	106.4 (3)	N(3)C(a6)C(m3)	124.9 (3)	125.5 (6)
O(1)Cl(1)O(3)	106.4 (2)	109.6 (3)	C(m3)C(a6)C(b6)	124.2 (3)	124.7 (6)
O(1)Cl(1)O(4)	108.2 (2)	108.6 (3)	N(4)C(a7)C(b7)	109.6 (3)	109.3 (5)
O(2)Cl(1)O(3)	110.5 (2)	110.3 (3)	N(4)C(a7)C(m3)	124.6 (3)	126.7 (6)
O(2)Cl(1)O(4)	111.5 (2)	110.3 (3)	C(m3)C(a7)C(b7)	125.8 (3)	124.1 (6)
O(3)Cl(1)O(4)	110.8 (2)	111.4 (3)	N(4)C(a8)C(b8)	110.6 (3)	109.1 (6)
C(a1)N(1)C(a2)	106.1 (3)	106.8 (5)	N(4)C(a8)C(m4)	124.5 (3)	125.3 (6)
C(a3)N(2)C(a4)	106.1 (3)	107.3 (5)	C(m4)C(a8)C(b8)	124.8 (3)	125.6 (6)
C(a5)N(3)C(a6)	105.9 (3)	107.0 (5)	C(a1)C(b1)C(b2)	107.2 (3)	106.8 (6)
C(a7)N(4)C(a8)	105.9 (3)	107.5 (5)	C(a2)C(b2)C(b1)	106.4 (3)	107.4 (6)
N(1)C(a1)C(b1)	109.4 (3)	109.4 (6)	C(a3)C(b3)C(b4)	107.1 (3)	107.1 (6)
N(1)C(a1)C(m4)	125.0 (3)	125.5 (6)	C(a4)C(b4)C(b3)	107.0 (3)	106.8 (6)
C(b1)C(a1)C(m4)	125.5 (3)	125.1 (6)	C(a5)C(b5)C(b6)	106.8 (3)	108.1 (6)
N(1)C(a2)C(b2)	110.6 (3)	109.5 (6)	C(a6)C(b6)C(b5)	106.8 (3)	106.1 (6)
N(1)C(a2)C(m1)	125.0 (3)	125.4 (6)	C(a7)C(b7)C(b8)	106.8 (3)	107.8 (6)
C(b2)C(a2)C(m1)	124.3 (3)	125.1 (6)	C(a8)C(b8)C(b7)	107.0 (3)	106.3 (6)
C(a2)C(m1)C(a3)	124.6 (3)	125.1 (6)	C(14)C(13)C(18)	119.0 (3)	117.3 (6)
C(a2)C(m1)C(1)	116.9 (3)	118.4 (6)	C(m3)C(13)C(18)	122.4 (3)	121.5 (6)
C(a3)C(m1)C(1)	118.3 (3)	116.4 (5)	C(m3)C(13)C(14)	118.6 (3)	121.2 (6)
C(a5)C(m2)C(a4)	123.8 (3)	125.6 (6)	C(13)C(14)C(15)	120.6 (4)	121.3 (6)
C(a5)C(m2)C(7)	118.7 (3)	117.5 (5)	C(14)C(15)C(16)	119.8 (4)	120.1 (6)
C(a4)C(m2)C(7)	117.5 (3)	116.9 (5)	C(15)C(16)C(17)	120.2 (3)	120.1 (6)
C(a7)C(m3)C(a6)	125.7 (3)	123.8 (6)	C(16)C(17)C(18)	120.2 (4)	119.6 (6)
C(a7)C(m3)C(13)	118.7 (3)	117.3 (6)	C(13)C(18)C(17)	120.1 (3)	121.6 (6)
C(a6)C(m3)C(13)	115.4 (3)	118.9 (6)	C(20)C(19)C(24)	118.9 (3)	118.0 (6)
C(a1)C(m4)C(a8)	125.5 (3)	124.7 (6)	C(24)C(19)C(m4)	119.4 (3)	120.0 (6)
C(a1)C(m4)C(19)	116.3 (3)	118.4 (6)	C(20)C(19)C(m4)	121.6 (3)	122.0 (6)
C(a8)C(m4)C(19)	118.1 (3)	116.9 (5)	C(19)C(20)C(21)	120.6 (3)	121.1 (6)
C(6)C(1)C(2)	119.0 (3)	119.1 (6)	C(20)C(21)C(22)	119.9 (3)	120.3 (7)
C(6)C(1)C(m1)	118.7 (3)	121.8 (6)	C(21)C(22)C(23)	120.1 (3)	119.7 (6)
C(2)C(1)C(m1)	122.2 (3)	119.1 (6)	C(22)C(23)C(24)	120.0 (3)	120.8 (6)
C(1)C(2)C(3)	120.0 (4)	119.8 (6)	C(19)C(24)C(23)	120.3 (3)	120.1 (6)
C(2)C(3)C(4)	119.8 (4)	120.2 (6)	C(9)C(10)C(11)	120.4 (3)	120.2 (6)
C(3)C(4)C(5)	120.6 (4)	120.2 (6)	C(10)C(11)C(12)	119.9 (3)	120.1 (7)
C(4)C(5)C(6)	119.9 (4)	120.2 (6)	C(7)C(12)C(11)	120.4 (3)	119.8 (6)
C(5)C(6)C(1)	120.7 (4)	120.6 (6)	Cl(2)C(25)Cl(3)	112.5 (2)	113.3 (5)
C(8)C(7)C(12)	118.5 (3)	119.5 (6)	Cl(4)C(26)Cl(5)	111.6 (3)	112.8 (6)
C(8)C(7)C(m2)	121.1 (3)	120.1 (6)	ZnO(1)Cl(1)	127.4 (2)	124.6 (3)
C(12)C(7)C(m2)	120.4 (3)	120.4 (6)			
C(7)C(8)C(9)	120.6 (3)	119.9 (6)			
C(8)C(9)C(10)	120.2 (4)	120.5 (6)			

Table VI. Comparison of Structural Parameters of the Crystalline Phases of $[Zn(TPP)OClO_3]$

param	form 1	form 2	β phase
Ph dihedral angles w/core[a]	50.9, 47.5, 52.4, 54.1	56.3, 61.2, 47.0, 44.5	44.3, 63.0, 52.2, 50.6
av abs disp,[b] C_m	12 (6)	6 (3)	2 (1)
av abs disp,[b] C_b	35 (6)	40 (4)	38 (7)
max C_b[b]	44	48	45
mean plane separation[c]	3.57	3.64	3.70
Ct···Ct[c]	4.823	5.135	6.539
lateral shift[c]	3.24	3.63	5.32
Ct position[d] (x,y,z)	2.90, −1.56, −3.53	3.34, −1.24, −3.70	4.13, −3.34, −3.81
Zn···Ct[c]	0.23	0.26	0.35
Zn–O[c]	2.129 (3)	2.139 (4)	2.079 (8)
dihedral angle N–Zn–O–Cl[a]	4.2	2.7	0.5
ref	this work	this work	9

[a] Value in deg. [b] Value in Å × 10^2. [c] Value in Å. [d] Orthogonalized coordinates in Å; see Figure 6.

stronger π–π interaction) leads to smaller zinc displacements and longer Zn–O bond distances. A similar effect resulting from a π-arene–porphyrin interaction in a five-coordinate Mn(III) complex has recently been noted.[22] In effect, the structural consequence of the π–π interaction on the coordination group of the central metal ion is similar to that of an additional weakly coordinated axial ligand. The out-of-plane displacements of zinc in forms 1 and 2 are distinctly smaller than those observed for all[23] five-coordinate zinc(II) porphyrinates having a neutral axial donor.

Figures 3 and 4 summarize average values for the various chemical bond lengths and angles in porphyrin cores. Close agreement between the two forms is evident and is also found for the averaged parameters of the β phase. The perchlorate ligand orientation with respect to the porphinato core is quite similar in all three forms of the molecule. In each, the Zn–O–Cl plane

(22) Williamson, M. M.; Hill, C. L. *Inorg. Chem.* **1987**, *26*, 4155–4160.
(23) Barkigia, K. M.; Fajer, J.; Spaulding, L. D.; Williams, G. J. B. *J. Am. Chem. Soc.* **1981**, *103*, 176–181. Bobrik, M. A.; Walker, F. A. *Inorg. Chem.* **1980**, *19*, 3283–3290. Collins, D. M.; Hoard, J. L. *J. Am. Chem. Soc.* **1970**, *92*, 3761–3771. Cullen, D. L.; Meyer, E. F. *Acta Crystallogr., Sect B* **1976**, *B32*, 2259–2269. Spaulding, L. D.; Andrews, L. C.; Williams, G. J. B. *J. Am. Chem. Soc.* **1977**, *99*, 6918–6922. Brennan, T. D.; Scheidt, W. R. *Acta Crystallogr., Sect. C* **1988**, *C44*, 478–482.

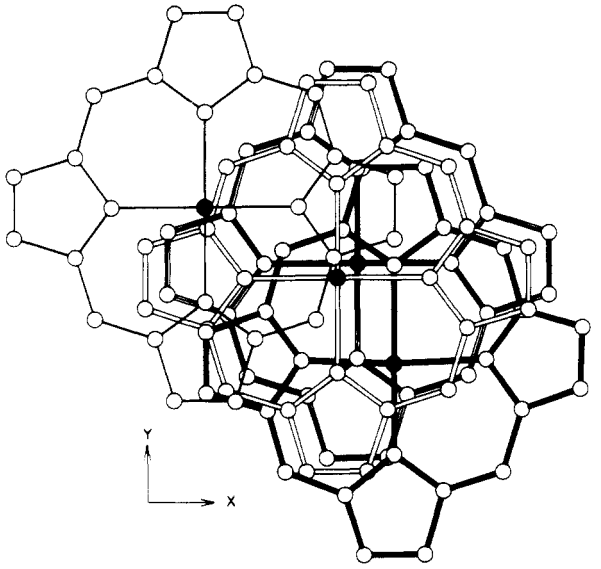

Figure 6. Schematic depiction of the $\pi-\pi$ interaction in the three structurally characterized phases of [Zn(TPP•)($OClO_3$)]. All dimer pairs are referred to a common origin molecule illustrated in the upper left-hand side. This molecule is drawn with single line bonds and is closest to the viewer. The second molecule of the dimer pairs are all in roughly the same plane away from the viewer. Owing to the nonplanar nature of the three separate cores, these molecules may appear to interpenetrate each other. The second molecule of each pair is then depicted as follows (progression to the right): form 1 is shown with two-line bonds, form 2 is shown with three-line bonds, and the β phase is shown with heavy bonds. The coordinate system used in the comparisons of Table VI is also shown.

is almost exactly parallel to a coordinate plane defined by N–Zn–O. Exact values are given in Table VI. This bisecting position of the perchlorate ligand serves to minimize nonbonded interactions between uncoordinated oxygen atoms and porphinato core atoms. A similar orientation of the perchlorate ligand is observed in [Fe(TPP)($OClO_3$)],[24] [Fe(OEP)($OClO_3$)],[25] and [Mg(TPP•)($OClO_3$)].[26] As expected, the coordinated O–Cl bond distance is longer than the other three O–Cl bonds (Table IV).

Hydrogen atom positions were experimentally defined in both structures. Both were well-behaved during the course of the least-squares refinement. The averaged values for the hydrogen atom bond parameters are C_b–H = 0.92 (5) (0.85 (9)) Å and C(phenyl)–H = 0.91 (4) (0.89 (8)) Å for form 1 (form 2). In interesting feature, which we have noted previously,[27] is the inequivalence of the bond angles involving the hydrogen atoms of the β-pyrrole carbon atoms. The C_a–C_b–H_b angles average to 124.1 (16) (123.6 (32))° while the C_b–C_b–H_b angles are substantially larger at 128.9 (16) (129.1 (31))°. We suggested that the inequivalence in the two angles serves to increase the $H_b\cdots H_b$ separation on any given pyrrole ring; the independent observation of similar differences in both of these structures strengthens this interpretation.

That both crystalline forms 1 and 2 exhibit identical solid-state stoichiometries naturally leads to the question of why both form under similar, if not identical, conditions. An examination of the packing of the molecules within their respective unit cells, shown in Figures S4 and S5 of the supplementary material, does not reveal any simple answers. An examination of the cell-packing diagrams shows that the dimers have different orientations with respect to the monoclinic *b* axis, and of course, there are the small

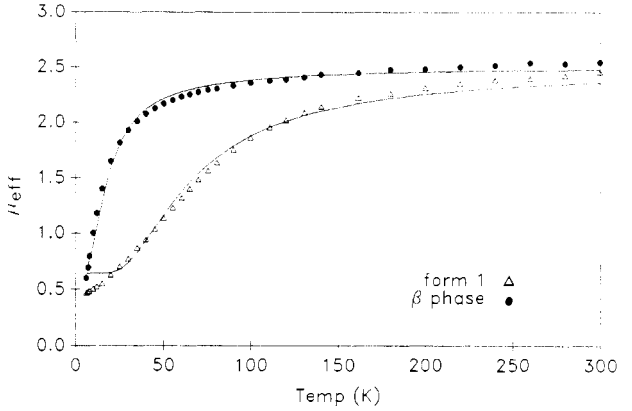

Figure 7. Magnetic moments per dimeric unit for form 1 of [Zn(TPP•)$OClO_3$]·$2CH_2Cl_2$ (Δ) and the β phase of [Zn(TPP•)($OClO_3$)] (●) versus temperature. The solid lines are least-squares theoretical fits with $J = -54.1$ cm^{-1}, $g = 2.05$, and $\chi_{imp} = 4.3\%$ and $J = -14.7$ cm^{-1}, $g = 2.03$, and $\chi_{imp} = 5\%$, respectively.

differences in the dimer interactions. The greater abundance of form 1 over form 2 and its slightly greater packing density (1.542 g/cm^3 vs 1.519 g/cm^2 at 118 K) suggests that form 1 might be thermodynamically favored. Both phases, however, appear unstable with respect to crystal desolvation at ambient conditions. The dichloromethane solvate molecules do not appear to have any obvious role in defining the two solid-state structures but rather simply are filling space in the lattices. The several other, less characterized phases are all apparently lattice-solvated species.

The fact that two more π-cation radicals are found to have dimeric solid-state structures again empirically emphasizes the strong driving force toward dimerization for this class of molecule. We presume that this phenomenon arises from the enhanced stability of delocalization of the radical electrons over both porphyrin rings as suggested by the interring magnetic coupling (vide infra). This leads us to speculate that a possible reason for the observation of the large number of crystalline phases of [Zn(TPP•)($OCLO_3$)] is that each crystalline phase represents a slightly different dimeric structure. This would be consistent with the motion that structures with similar overlap areas, but slightly different relative ring orientations, may not be very different in total energy. As has been pointed out in the Scheidt and Lee review,[8] the dimeric structures of porphyrins, both radical and neutrals, display three different "regions of stability" that can be defined by a single parameter (lateral shift). Within each stability group a number of differing specific relative orientations are found. In this context, we note that we have also prepared the water-ligated radical [Zn(TPP•)(OH_2)]ClO_4 and analyzed its crystal and molecular structure.[28] Although the structural analysis has been hampered by solvent disorder, we note that this species also exhibits dimer formation. The structural parameters of this dimer are intermediate to the two radical species reported here (forms 1 and 2).

Magnetic Studies. Magnetic susceptibility measurements on the dichloromethane solvated forms of [Zn(TPP•)($OClO_3$)] were problematic. For all phases except form 1, we were unable to accumulate sufficient quantities by manual crystal selection techniques to be confident of sample purity or to test for data reproducibility. Sample grinding and packing, necessary to prevent possible crystallite orientation in the magnetic field, probably accelerates the egress of lattice solvent that is characteristic of aged samples. For this reason, crystalline samples were kept at subambient temperatures except for the sorting and mounting operations. After data were collected from 6 to 300 K, repeat measurements typically showed a few percent increase in the molar susceptibility at lower temperatures indicating a weakening of antiferromagnetic coupling. We ascribe this to solvent loss and

(24) Reed, C. A.; Mashiko, T.; Bentley, S. P.; Kastner, M. E.; Scheidt, W. R.; Spartalian, K.; Lang, G. *J. Am. Chem. Soc.* **1979**, *101*, 2948–2958.
(25) Masuda, H.; Taga, T.; Osaki, K.; Sugimoto, H.; Yoshida, Z. I. *Inorg. Chem.* **1980**, *19*, 950–955.
(26) Barkagia, K. M.; Spaulding, L. D.; Fajer, J. *Inorg. Chem.* **1983**, *22*, 349–351.
(27) Scheidt, W. R.; Haller, K. J.; Hatano, K. *J. Am. Chem. Soc.* **1980**, *102*, 3017–3021.

(28) Crystal data: triclinic: $a = 11.96$ Å, $b = 13.82$ Å, $c = 14.53$ Å, $\alpha = 76.80°$, $\beta = 72.89°$, $\gamma = 74.65°$, $V = 2183$ Å^3 (118 K). Additional work on neutral ligand π-cation-radical species is in progress.

lattice breakup from grinding, thermal stress, and ambient temperature exposure at the end of the data collection procedure.

The magnetic susceptibility data for form 1 and for the unsolvated β phase are displayed graphically in Figure 7. The plotted data are expressed in terms of the magnetic moment per dimer and the room-temprature moments (2.46 and 2.55 μ_B, respectively) are seen to have values close to the spin-only value of 2.45 μ_B (the square root of the sum of the squares of individual $S = {}^1/_2$ moments of 1.73 μ_B). These values, and those of all the higher temperature points, are, of course, quite sensitive to the value of the diamagnetic correction used: -898 and -806×10^{-6} cgsu/mol of dimer, respectively, for form 1 and the β phase. These values are based on Pascal's constants[29] and do not include the constitutive correction for TPP suggested by Eaton and Eaton[30] because doing so leads to unrealistically high moments ($\sim$2.8 μ_B). It is unknown what the constitutive correction for the TPP$^{\bullet}$ radical cation should be, but our current work suggests it may be lower than that of TPP itself. The marked decrease in magnetic moments as a function of decreasing temperature seen in Figure 7 reveals antiferromagnetic coupling in both systems. It is qualitatively evident that spin coupling is stronger in form 1 than in the β phase. A quantitative treatment leads to the theoretical fits displayed in the same figure. Fitting parameters are given in the figure caption. The derived values of the isotropic exchange coupling parameter J (in terms of the $-2J$ spin Hamiltonian) are -54 and -15 cm^{-1} for form 1 and the β phase, respectively. From our experience with the theoretical fitting variables, the uncertainty of the precise diamagnetic correction, and the sample aging difficulties with form 1, we estimate these values are reliable to within about 10%. Particularly because of the aging problem with the dichloromethane solvate, the $|-J|$ value for form 1 should be considered a lower limit. For the purposes of the present study, the qualitatively conclusion is probably the most important one. Antiferromagnetic coupling is significantly stronger in form 1 than in the β phase, and this correlates with the relative extent of the dimer interactions seen in the crystal structures. Table VI lists the dimensional criteria discussed earlier for describing the extent of dimer interaction. Although it is too early to judge which is the most important for magnetic coupling, it seems likely that both the interplanar separation and the degree of lateral overlap are critical.

Conclusions. The apparently quite strong driving force toward pairwise association of metallotetraphenylporphyrin π-cation-radical species is further demonstrated in these studies. Dimer formation has significant effects on the molecular structure, leading to an unusual saddle-shaped core conformation. Solid-state dimer formation also leads to antiferromagnetic coupling between the ring radicals and the extent of the coupling appears to be quite sensitive to the extent of porphyrin core overlap. Since spin coupling is insufficient to produce diamagnetism at room temperature, the present work supports the partitioning of intra- and intermolecular spin coupling effects previously made in iron(III) and copper(II) porphyrin radicals.[3,4]

Acknowledgment. We thank Drs. R. H. Blessing and G. DeTitta of the Medical Foundation of Buffalo for providing us the Fortran code of the profile analysis software and Dr. P. D. W. Boyd of the University of Auckland, New Zealand, for magnetic susceptibility fitting programs. We thank Ted Brennan for work on the structure of $[Zn(TPP^{\bullet})(OH_2)]ClO_4$. We gratefully acknowledge support of this research by the National Institutes of Health (Grants GM-38401 to W.R.S. and GM-23851 to C.A.R).

Registry No. $[Zn(TPP^{\bullet})(OClO_3)]\cdot 2CH_2Cl_2$, 119946-95-1.

Supplementary Material Available: Figure S1 (an edge-on view of the dimer of form 2), Figures S2 and S3 (overlap diagrams of the porphyrin core pairs (including phenyl rings)), Figures S4 and S5 (cell-packing diagrams), Tables SI and SII (magnetic susceptibility data for form 1 and the β phase, respectively), Table SIII (complete crystallographic details), and Tables SIV and SV (thermal parameters for the atoms of $[Zn(TPP^{\bullet})(OClO_3)]$ of forms 1 and 2, respectively) (11 pages); listings of observed and calculated structure factor amplitudes (×10) for the two structures (42 pages). Ordering information is given on any current masthead page.

(29) Boudreaux, E. A.; Mulay, L. N. *Theory and Applications of Molecular Paramagnetism*; Wiley: New York, 1976.
(30) Eaton, S. S.; Eaton, G. R. *Inorg. Chem.* **1980**, *19*, 1096–1098.

Contribution from Chemistry Department A, Technical University of Denmark, DK-2800 Lyngby, Denmark, Institute of Chemical Engineering and High Temperature Processes, University of Patras, Gr-26110 Patras, Greece, and Chemistry Department B, Technical University of Denmark, DK-2800 Lyngby, Denmark

Crystal Structure and Infrared and Raman Spectra of $K_4(VO)_3(SO_4)_5$

R. Fehrmann,[1a] S. Boghosian,[1b,c] G. N. Papatheodorou,[1b,c] K. Nielsen,[1d] R. W. Berg,*[,1a] and N. J. Bjerrum[1a]

Received June 17, 1988

Blue crystals of $K_4(VO)_3(SO_4)_5$ suitable for X-ray structure determination have been obtained from solutions of V_2O_5 in molten $K_2S_2O_7$ under a SO_2/N_2 gas mixture. Lowering the temperature from the range 470–450 °C to the range 440–420 °C causes small crystals to precipitate after several hours. The compound crystallizes in the monoclinic space group $P2_1/n$ (No. 14) with $a = 8.746$ (2) Å, $b = 16.142$ (2) Å, $c = 14.416$ (2) Å, and $\beta = 106.81$ (1)° at 18 °C and $Z = 4$. It contains three different distorted VO_6 octahedra and five distorted SO_4 tetrahedra. The central vanadium atoms have a short bond to one oxide ion, four longer bonds to the oxygens of four sulfate groups, and an especially long axial bond to a fifth SO_4^{2-}. The vanadium environment is similar to what is found for other vanadyl compounds. The structure has five different sulfate groups, with three of the four sulfate oxygens bridging the vanadiums in a complicated packing pattern. Principal component analyses were performed to examine structure correlations among different sulfate and VO_6 groups. Infrared and Raman spectra of the compound have been recorded and interpreted.

Introduction

The chemistry of the molten V_2O_5–$KHSO_4$–$K_2S_2O_7$ system in contact with $SO_2/O_2/SO_3/N_2$ is being investigated due to its importance as a catalyst for the production of sulfuric acid. The investigations so far include a study[2] of the pure solvent system $KHSO_4$–$K_2S_2O_7$ and the V_2O_5–$K_2S_2O_7$–K_2SO_4 system dilute in vanadium[3] and studies[4–6] of this system at 400–500 °C, including

(1) (a) Chemistry Department A, Technical University of Denmark. (b) University of Patras. (c) Visiting Scientist at the Technical University of Denmark in 1985. (d) Chemistry Department B, Technical University of Denmark.
(2) Fehrmann, R.; Hansen, N. H.; Bjerrum, N. J. *Inorg. Chem.* **1983**, *22*, 4009.
(3) Hansen, N. H.; Fehrmann, R.; Bjerrum, N. J. *Inorg. Chem.* **1982**, *21*, 744.
(4) Fehrmann, R.; Gaune-Escard, M.; Bjerrum, N. J. *Inorg. Chem.* **1986**, *25*, 1132.

0020-1669/89/1328-1847$01.50/0